Doped Kondo chain, a heavy Luttinger liquid

Ilia Khait[a,1], Patrick Azaria[a,b], Claudius Hubig[c], Ulrich Schollwöck[c], and Assa Auerbach[a]

[a]Physics Department, Technion, 32000 Haifa, Israel; [b]Laboratoire de Physique Théorique des Liquides, Université Pierre et Marie Curie, 75252 Paris, France; and [c]Arnold Sommerfeld Center for Theoretical Physics, Ludwig-Maximilians-Universität München, 80333 Munich, Germany

Edited by Piers Coleman, Rutgers University, Piscataway, NJ, and accepted by Editorial Board Member Zachary Fisk April 6, 2018 (received for review November 8, 2017)

The doped 1D Kondo Lattice describes complex competition between itinerant and magnetic ordering. The numerically computed wave vector-dependent charge and spin susceptibilities give insights into its low-energy properties. Similar to the prediction of the large N approximation, gapless spin and charge modes appear at the large Fermi wave vector. The highly suppressed spin velocity is a manifestation of "heavy" Luttinger liquid quasiparticles. A low-energy hybridization gap is detected at the small (conduction band) Fermi wave vector. In contrast to the exponential suppression of the Fermi velocity in the large-*N* approximation, we fit the spin velocity by a density-dependent power law of the Kondo coupling. The differences between the large-*N* theory and our numerical results are associated with the emergent magnetic Ruderman–Kittel–Kasuya–Yosida interactions.

heavy fermions | Kondo lattice | magnetism | strongly correlated systems

The Kondo Lattice (KL) (1–3) describes itinerant conduction electrons Kondo-coupled to localized spins in each unit cell by an $SU(2)$ (special unitary group of degree 2) symmetric magnetic interaction. The KL has been intensively studied as the microscopic model of heavy fermion (HF) metals in rare earth compounds. Nevertheless, much remains unknown about its low-energy correlations.

The large-N limit of the $SU(N)$ model was worked out long ago (4–7). It describes a Fermi liquid of hybridized conduction and valence electrons with a large Fermi surface. It includes conduction electrons and localized spins as itinerant fermions in agreement with Luttinger's theorem (8–10). Signatures of the large Fermi surface were found numerically in one dimension (11) and experimentally in HF compounds (12, 13). The large-N theory predicts an exponentially small (in inverse Kondo coupling) Fermi velocity, which resembles the scaling of the single impurity Kondo temperature (3). However, the validity of the large-N approximation for the physical $N=2$ KL has been severely challenged. Intersite magnetic interactions, named RKKY (Ruderman–Kittel–Kasuya–Yosida) (14), emerge at second order in the Kondo coupling and at order $1/N^2$ (15), but they are neglected in the large-N approximation. RKKY interactions may well destabilize the HF metal by magnetic ordering (2) or at least change its low-energy scales and correlations (16). If a Fermi liquid phase is indeed found at weak coupling, the crucial question is as follows: how does the spin velocity (i.e., the renormalized Fermi velocity of the spin mode) scale with the Kondo coupling for $N=2$?

In 1D, KL has been notoriously resistant to treatments by exact solutions, bosonization, quantum Monte Carlo, and field theory, especially away from half-filling.[‡]

Its phase diagram (Fig. 1) has been determined numerically (11, 20–27) using exact diagonalization and Density Matrix Renormalization Group (DMRG) (28). From the analysis of spin and charge density Friedel oscillations and the large-N approach (29), a Tomonaga–Luttinger Liquid (30, 31) (TLL) phase was hypothesized with a large Fermi surface (9) and a small Luttinger interaction parameter [although there is some controversy regarding the size of the Fermi surface that remained (32, 33)]. The importance of carefully treating the RKKY interactions was shown in recent works (34, 35) on the anisotropic KL model using bosonization. They obtained an easy-plane spiral phase, with broken Z_2 symmetry, and an easy axis phase. Both phases exhibit collective fluctuations at twice the small Fermi wave vector. The $SU(2)$ symmetric model analyzed here, however, is a quantum critical point between these phases. It has no broken symmetry, and massless fermions are at a large Fermi wave vector.

In this paper, we provide comprehensive numerical proof for the existence of a TLL. We probe this phase by computing the wave vector-dependent charge and spin susceptibilities. These response functions allow us to measure the low-energy momentum and velocity scales. Their singularities can be described by a Heavy Tomonaga–Luttinger Liquid (HTLL), which is characterized by gapless spin and charge modes at the large Fermi wave vector. The Luttinger interaction parameter is much smaller than unity, and the spin velocity is highly suppressed relative to the charge velocity.[§] For the values of n_c calculated, the spin velocity fits power laws of the Kondo coupling in contrast to the exponential behavior predicted by the large-N theory (29). We also detect a low-energy charge gap at twice the small (conduction electrons') Fermi wave vector. This gap is qualitatively consistent with the hybridization gap expected by the large-N approach. We present the numerical calculation of its dependence on the interaction strength, which shows power law behavior. The difference between the numerical results and the large-N approximation is associated with the effects of RKKY interactions. The 1D

Significance

The large effective electron mass observed in rare-earth "heavy fermion" metals, such as $CeAl_3$ and $CeCu_6$, has challenged theorists since the discovery of the effect in 1975. In particular, the popular theory that explains the electron mass enhancement neglects important emergent magnetic interactions, which could destroy the heavy fermion phase by magnetic ordering. Here, we investigate in great detail the effect of these magnetic interactions in the 1D Kondo Lattice model, which approximates such metals. Surprisingly, we find that magnetism helps to stabilize the heavy fermion metal, albeit with different energy scales than previously predicted. These insights may help us understand the Kondo Lattice and heavy fermions in higher dimensions.

Author contributions: I.K., P.A., and A.A. designed research; I.K., P.A., and A.A. performed research; C.H. and U.S. contributed a numerical tool; and I.K., P.A., C.H., U.S., and A.A. wrote the paper.

The authors declare no conflict of interest.

This article is a PNAS Direct Submission. P.C. is a guest editor invited by the Editorial Board.

[1]To whom correspondence should be addressed. Email: iliakh@tx.technion.ac.il.

This article contains supporting information online at www.pnas.org/lookup/suppl/doi:10.1073/pnas.1719374115/-/DCSupplemental.

[‡]Indeed, in most of the bosonization approaches of the KL, an effective coupling J_H between the impurity spins is assumed. This is the Kondo–Heisenberg model (17–19). In this case, the renormalized mass, which is of the order of ${J_H}^{-1}$, is fixed and of order unity.

[§]Previous DMRG studies have detected a suppression of spin velocity and a large Fermi wave vector in the boundary Friedel oscillations (29). However, real space Friedel oscillations cannot easily resolve subdominant wave vectors' contributions.

KL at weak coupling, $J < t$, traditionally assumed that RKKY interactions dominate the low-energy physics and inhibit the Kondo effect, which produces heavy quasiparticles. However, our conclusion is that itineracy and RKKY work hand in hand to produce the HTLL, with a large Fermi wave vector, which bears resemblance to HF states in higher dimensions.

Model

We study the $SU(2)$ 1D KL model:

$$\mathcal{H} = -t \sum_{i,s} c^{\dagger}_{i,s} c_{i+1,s} + \text{H.c} + J \sum_{i} \vec{S}_i \cdot \vec{s}_i. \qquad [1]$$

J is the Kondo interaction. c_{is} annihilates an electron at position $i = 1 \ldots L$ with z spin s; $s^{\alpha}_i = \frac{1}{2} \sum_{ss'} c^{\dagger}_{is} \sigma^{\alpha}_{ss'} c_{is'}$, S^{α} are spin-half operators of the conduction electrons and localized f spins, and $\sigma^{\alpha}, \alpha = x, y, z$ are Pauli matrices. The conduction electron number $N_c = n_c L$ defines the "small" Fermi wave vector $k_F = \frac{\pi}{2} n_c$. The "large" (Luttinger theorem) Fermi wave vector is $k^{\star}_F = k_F + \frac{\pi}{2}$.

The phase diagram in the n_c, J/t plane is shown in Fig. 1. Here, we avoid the ferromagnetic regions (FMs) FM1 and FM2 and choose our parameters to be well within the weak-coupling paramagnetic regime. Note that, according to the large-N theory (Eq. **11**), weak coupling is defined by $0 < \frac{J}{t} \ll 4\pi \sin(k^{\star}_F)$.

Luttinger Parameters and Susceptibilities

The uniform spin and charge susceptibilities are given by differentiating the ground-state energy $E_0(L, N_c, M)$, where $M = \sum_i (S^z_i + s^z_i)$ is the conserved magnetization:

$$\chi_s(L) = \frac{1}{L} \left(\frac{\partial^2 E_0}{\partial M^2} \right)^{-1}, \quad \chi_c(L) = \frac{1}{L} \left(\frac{\partial^2 E_0}{\partial N_c^2} \right)^{-1}. \qquad [2]$$

By the TLL theory, these are related to the spin and charge velocities by

$$v_s = \chi_s^{-1}/(2\pi), \quad v_c = \chi_c^{-1} K/(2\pi), \qquad [3]$$

respectively, where K is the Luttinger interaction parameter. In a TLL theory, the spin and charge density Friedel oscillations near the boundaries are given to leading order by (20, 36)

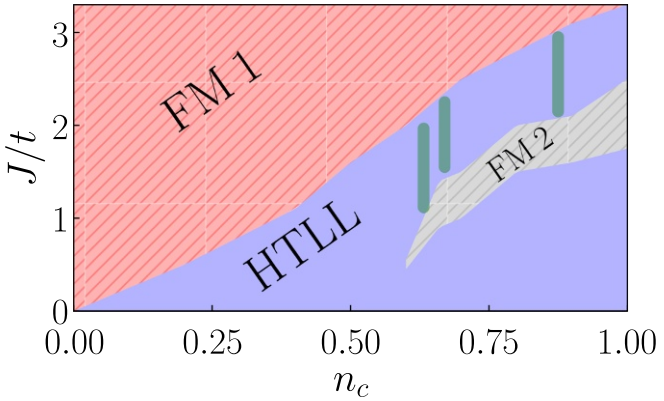

Fig. 1. Schematic phase diagram of the KL model in one dimension; n_c is the conduction electron density, and J/t is the dimensionless Kondo coupling constant. FM1 (11) and FM2 (20–22) are shown. The paramagnetic phase (blue) is characterized as an HTLL. The DMRG calculations reported here are carried out at densities $n_c = 0.6, 0.67,$ and 0.875 marked with thick vertical green lines.

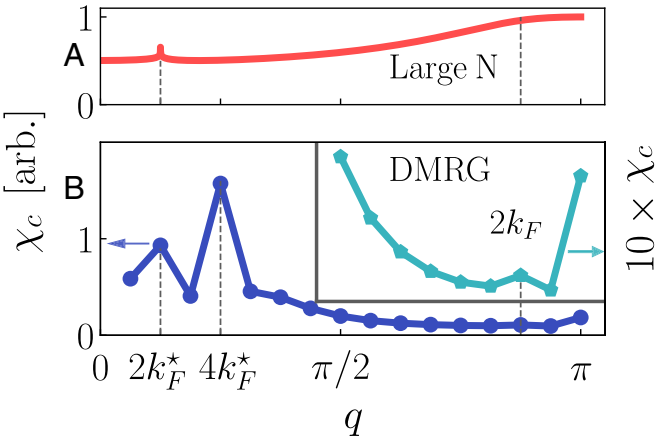

Fig. 2. Charge susceptibility vs. wave vector for $n_c = 0.875, J/t = 2.5$. (*A*) large-*N* approximation. (*B*) DMRG calculation. $k^{\star}_F$ denotes the large Fermi surface wave vector. Finite-field scaling of DMRG reveals divergent peaks at $2k^{\star}_F$ and $4k^{\star}_F$ as expected for a TLL. *B*, *Inset* shows a nondivergent peak at twice the small Fermi wave vector $2k_F$, which is attributed to the inverse of the hybridization gap $2r_0$ depicted in Fig. 6. arb, arbitrary units.

$$\langle (S^z_i + s^z_i) \rangle = B_1 \cos(2k^{\star}_F x)\, x_i^{-K} \qquad [4]$$

and

$$\sum_s \langle c^{\dagger}_{is} c_{is} \rangle = A_1 \cos(2k^{\star}_F x_i)\, x_i^{-\frac{K+1}{2}} + A_2 \cos(4k^{\star}_F x_i)\, x_i^{-2K}, \qquad [5]$$

which allows us, in principle, to extract $k^{\star}_F$ and K. Other wave vectors are associated with smaller-amplitude oscillations, which are hard to extract from Eqs. **4** and **5**. Therefore, we use a complementary approach and calculate the susceptibilities by adding wave vector-dependent source terms to the Hamiltonian:

$$\mathcal{H}' = -h_q (S^z_q + s^z_q) - \mu_q \rho_q,$$

where S^z_q, s^z_q, and ρ_q are the lattice cosine transforms of the operators S^z_i, s^z_i, and ρ_i. The susceptibilities are obtained by differentiating the DMRG ground-state energies:

$$\chi_s(q) = -\frac{1}{L} \frac{\partial^2 E_0}{\partial h_q^2}, \quad \chi_c(q) = -\frac{1}{L} \frac{\partial^2 E_0}{\partial \mu_q^2}. \qquad [6]$$

To avoid finite lattice effects, we take h_q and μ_q to be larger than the respective finite size gaps.

Methods

We use open boundaries with $U(1)$[¶] (unitary group of degree 1) and $SU(2)$[#] DMRG (28). Lattice sizes were $L \leq 192$. We retain up to 5,500 states in the reduced density matrix; 28 sweeps were sufficient for good convergence. The DMRG relative truncation error was less than 10^{-8}.

Friedel spin density oscillations were found at twice the large Fermi wave vector $2k^{\star}_F = 2k_F + \pi$, in agreement with Luttinger's theorem. Due to the very low values of K, the signature of $2k^{\star}_F$ in the charge Friedel oscillations is too weak for detection (11, 23–27) (*SI Appendix*, Fig. S5).

The Luttinger parameter K was determined by measuring the power law singularities of the density operator n_q at $2k^{\star}_F$ and $4k^{\star}_F$. TLL theory yields the scaling relation (*SI Appendix* has a complete derivation):

$$n_q = -\frac{1}{L} \frac{\partial E_0}{\partial \mu_q} \sim \mu_q^{\frac{\Delta(q)}{2-\Delta(q)}}, \qquad [7]$$

[¶] Calculations were performed using the ITensor library.

[#] Calculations were performed using the SyTen library.

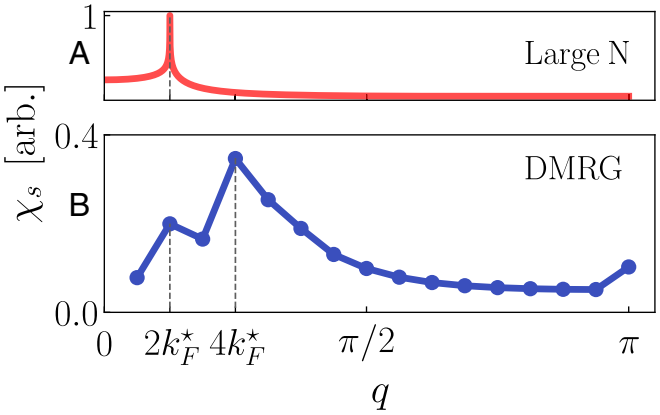

Fig. 3. Spin susceptibility vs. wave vector for $n_c = 0.875, J/t = 2.5$. (*A*) large-*N* approximation. (*B*) DMRG calculation. Finite-field scaling reveals a divergent peak at $q = 2k_F^\star$. arb, arbitrary units.

where $\Delta(q = 2k_F^\star) = \frac{K+1}{2}$ and $\Delta(q = 4k_F^\star) = 2K$ are the scaling dimensions of n_q at the two wave vectors $2k_F^\star$ and $4k_F^\star$. We find good agreement for the values of K extracted from Δ and from the charge density Friedel oscillations in Eq. **5**.

Results

We chose three fillings, $n_c = 0.6$, 0.67, and 0.875, with associated ranges of coupling constant J/t within the paramagnetic region (shown in Fig. 1). The lower values of J/t were limited by the rapid increase of ground-state entanglement, which approached the numerical limitations of our DMRG calculations.

The Friedel oscillations of the spin density are dominated by wave vector $2k_F^\star$. The charge density oscillations are dominated by the $4k_F^\star$ terms, since $K < 0.33$ (Eq. **5**). The subdominant $2k_F^\star$ oscillations were too weak for detection in the Friedel oscillations (36).

The wave vector-dependent charge and spin susceptibilities are depicted in Figs. 2 and 3, respectively. We note the detection of divergent peaks at $2k_F^\star$ in both spin and charge sectors, which firmly confirm the TLL phase with a large common Fermi wave vector $k_F^\star$. The charge sector shows a pronounced peak at $4k_F^\star$ as expected for small values of K.

In Fig. 4, the values of the Luttinger parameter $K(n_c, J/t)$ are depicted; we note a monotonic decrease as a function of J/t, signaling stronger repulsive interactions at weak coupling in agreement with earlier calculations by Shibata et al. (29).

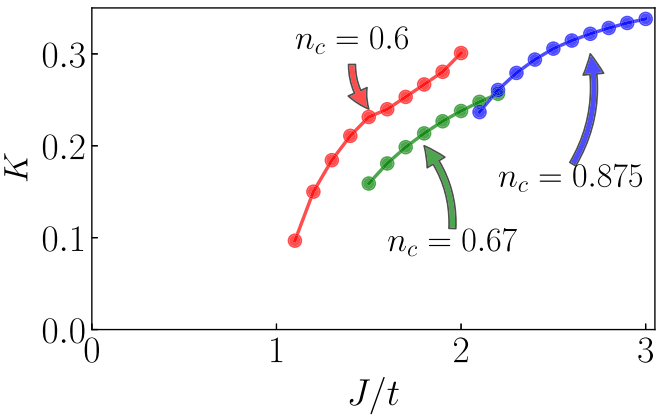

Fig. 4. Luttinger interaction parameter K along the three lines shown in Fig. 1. The values of $K \lesssim 0.33$ throughout the HTLL phase (in the text) indicate effects of strong repulsive interactions.

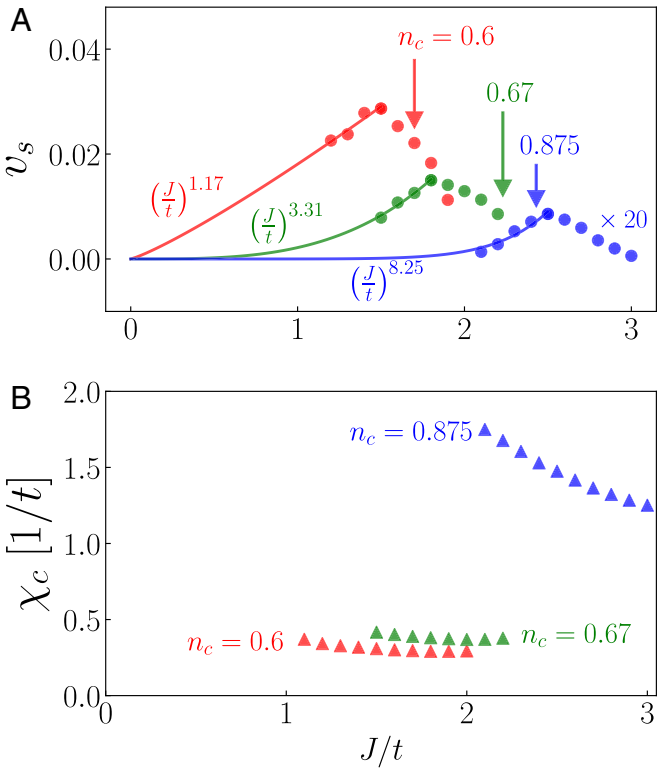

Fig. 5. (*A*) Spin velocity as a function of J/t at different fillings. Solid lines are power laws $v_s \sim A(n_c)(J/t)^{\alpha(n_c)}$. We note a significant increase of α and a decrease of A as n_c increases (*Discussion*). (*B*) Uniform ($q = 0$) charge susceptibility. Note a weaker dependence of χ_c on n_c and J/t than for the spin susceptibility (Fig. 7).

We compute the spin and charge velocities of the TLL by Eq. **3**. The spin velocity $v_s(J/t)$, as shown in Fig. 5*A*, is highly suppressed in the weak-coupling limit $J/t \ll 1$. This "heaviness" is the hallmark of HTLL phase. We can fit v_s to a power law $(J/t)^{\alpha(n_c)}$, where $1.1 < \alpha < 8.3$. The power α increases significantly as n_c approaches unity.

In Fig. 5*B*, we see that the charge susceptibility varies only moderately with J/t and n_c. For our parameters, the charge velocities v_c are at least an order of magnitude larger than the respective v_s.

Fig. 2*B* shows a nondiverging peak at twice the small Fermi wave vector, which is attributed to the inverse hybridization gap (*Discussion*). Clearly, this is the high-energy scale, much larger than the characteristic energy scales for which the HTLL is relevant. The appearance of the hybridization gap is shared by other fillings as well.

Large-*N* Approximation

The localized spins in Eq. **1** are represented by slave fermions:

$$S_i^\gamma = \frac{1}{2}\sum_{s,s'} f_{i,s}^\dagger \sigma_{ss'}^\gamma f_{i,s'}, \qquad [8]$$

which are subject to a constraint $\sum_s f_{i,s}^\dagger f_{i,s} = 1$. The large-*N* approximation yields an effective hybridized band structure, which is depicted in Fig. 6:

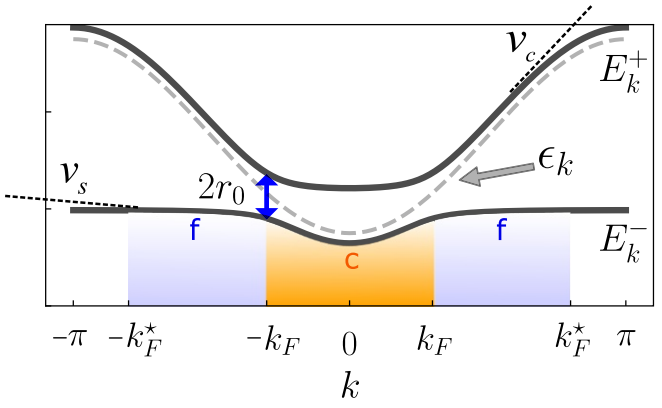

Fig. 6. Band structure of the large-*N* Hamiltonian. ϵ_k is the tight binding kinetic energy, $E_k^\pm$ are the hybridized bands, $2r_0$ is the hybridization gap. The shaded area denotes the occupied part of the Fermi surface. Blue-colored f and orange-colored c denote the f-character and c-character parts of the band, respectively. Note the suppression of the spin velocity v_s compared with the charge velocity given by v_c.

$$\mathcal{H}^{\text{Large}-\text{N}} = \sum_{ks} \epsilon_k c_{ks}^\dagger c_{ks} + r_0 c_{ks}^\dagger f_{ks} + \text{H.c} + \epsilon_f f_{ks}^\dagger f_{ks}$$
$$= \sum_{ks} E_k^\pm \alpha_{\pm,k,s}^\dagger \alpha_{\pm,k,s}. \quad [9]$$

The bare conduction electron band structure is $\epsilon_k = -2t\cos(k)$, and the large-*N* hybridized bands $E_k^\pm$ are

$$E_k^\pm = \frac{\epsilon_k + \epsilon_f}{2} \pm \sqrt{\left(\frac{\epsilon_k - \epsilon_f}{2}\right)^2 + r_0^2}. \quad [10]$$

ϵ_f and r_0 are variational parameters, which depend on J/t and n_c. Solving the mean field equations at weak coupling yields (37)

$$r_0^2 = \left(\frac{\epsilon_{k_F^\star} - \epsilon_{k_F}}{2\rho_0 \epsilon_{k_F^\star}}\right) e^{\frac{1}{\rho_0 J}}, \quad [11]$$

where $\rho_0 = \frac{1}{4\pi t \sin(k_F^\star)}$ is the (single-spin) conduction electron's density of states at the large Fermi wave vector. r_0^2 determines the Fermi velocity suppression as $v_F^\star = 2tr_0^2 \sin(k_F^\star)$, and r_0 yields the minimal hybridization gap at k_F. As shown in Fig. 6, the small Fermi wave vector k_F marks a sharp cross-over in the character of the quasiparticles from c to f fermions.

Discussion

The large-*N* theory effectively describes noninteracting fermions (in essence, a TLL with $K = 1$). Its spin and charge wave vector-dependent susceptibilities are compared with the DMRG in Figs. 2 and 3. Large-*N* theory exhibits a weak logarithmic singularity at $2k_F^\star$, while the DMRG exhibits a K-dependent power law divergence. The DMRG peak in $\chi_c(q)$ at $4k_F^\star$, absent in the large-*N* theory, is also associated with $K < 1$.

Similarities between large-*N* theory and the DMRG are as follows.

i) The ratio of charge to spin susceptibilities. In the large-*N* theory,

$$\frac{\chi_s}{\chi_c} = r_0^{-2} \propto e^{\frac{1}{\rho_0 J}}, \quad [12]$$

which follows from the dominance of the f fermions character at $k_F^\star$. The DMRG also obtains $\frac{\chi_s}{\chi_c} \gg 1$ throughout the studied parameter regime.

ii) In the large-*N* theory, the f fermions cannot contribute to the charge susceptibility. χ_c is completely determined by the conduction electrons susceptibility and is weakly dependent on the Kondo coupling. The DMRG results for χ_c are also weakly dependent on J/t, as shown in Fig. 5.

iii) The hybridized bands in the large-*N* theory predict a minimal hybridization gap at the small Fermi wave vector k_F (Fig. 6). This gap should be proportional to the square root of the spin velocity. The DMRG indeed finds a small peak at $2k_F$ (Fig. 2*B*, *Inset*). This peak can be interpreted as a signature of a hybridization gap at $\pm k_F$, albeit with a different parametric dependence on J/t than given by Eq. **12**. This qualitative feature is in support of a hybridized band description of the HTLL.

Differences between the large N and the DMRG results are especially noteworthy. As seen in Fig. 7, the variation of the spin velocity with the Kondo coupling is well-fit by power laws. The large-*N* predictions cannot be reconciled with the numerical data unless large renormalization factors are introduced into the exponent of Eq. **12**. While it is hard to distinguish between a power $v_s \propto (J/t)^\alpha$ and a general exponential function $e^{-F(n_c)t/J}$, it requires unjustifiably large renormalization factors $F(n_c)$, especially at lower fillings. In addition, we find that the hybridization gap scales weakly with the Kondo coupling compared with the high-power law suppression of the spin velocity (Fig. 5*A*). This differs from the large-*N* prediction (Eq. **12**).

Fig. 5*A* shows that the DMRG-obtained power laws α increase toward half-filling, $n_c \to 1$. The reason for the increase in $\alpha(n_c)$ is still uncertain, but it may be associated with the approaching phase transition into the Kondo insulator at $n_c = 1$, where both spin and charge modes are gapped (11).

Summary

Our DMRG results of the spin and charge wave vector-dependent susceptibilities establish the HTLL phase of the $N = 2$ KL model at weak coupling and away from half-filling. In addition, we find numerical evidence for hybridized band features revealed by a nondivergent peak of the wave vector-dependent charge susceptibility at precisely twice the small Fermi wave vector $2k_F$. Altogether, our results strongly support the fact that, at least in one dimension, the RKKY interactions do not destroy the heavy quasiparticles at $k_F^\star$ but "work with them" to produce the HTLL. At this point, it is worth commenting on recent works (34, 35) studying the anisotropic KL, where it was found that, in the presence of a strong easy-plane anisotropy (XXZ type),

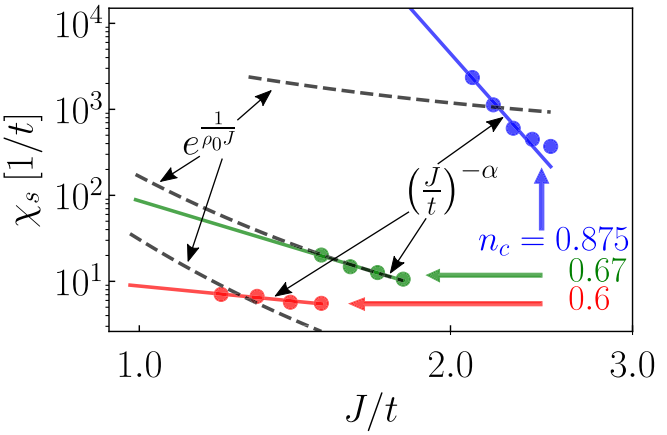

Fig. 7. Uniform spin susceptibility, which is related to the velocity of Fig. 5 via $\chi_s = 1/(2\pi v_s)$. Solid straight lines are a fits to power laws $\chi_s \propto (J/t)^{-\alpha}$. Dashed lines are fits to the large-*N* theory $\chi_s^{\text{Large}-\text{N}} \propto e^{\frac{1}{\rho_0 J}}$.

RKKY is responsible for $2k_F$ ordering of the f spins and predominates over the Kondo screening. Although this leads to interesting physics, the latter scenario is not extended to the isotropic limit. Indeed, in the $SU(2)$ invariant case, quasilong-range helical ordering is likely to be destroyed by quantum fluctuations (e.g., in the spin one-half $J_1 - J_2$ spin chain) (38). We believe that, in the isotropic limit, RKKY induces $2k_F$ fluctuations of the f spins that couple to those of the conduction electrons, resulting in the opening of the hybridization gap [which is proportional to $\chi_c^{-1}(2k_F)$]. This scenario is consistent with our numerical results. Future calculations of spectral functions could explore the scaling of the hybridization gap by, for example, time-dependent DMRG (39, 40).

We note that, in commensurate fillings [i.e., half-filling (11) and quarter-filling (41)], a charge gap was observed. At quarter-filling, the f spins open a gap and dimerize. We conclude that the RKKY wave vectors play an important role in the competition between the formation of the decoupled f-spin gap and the formation of the hybridization gap.

The scaling of the Luttinger parameters as a function of the Kondo coupling can serve as a useful guide for future work. Specifically, in any analytical approach, two parametrically different energy scales are expected to emerge in the HTLL phase: the spin velocity v_s and the hybridization gap at $2k_F$. Sorting out the interplay between dimerization and $2k_F$ hybridization remains as a challenge to theory. We hope that future experimental realizations of the KL in wires and cold atom systems may also shed light on these issues.

Lessons learned here could be relevant to the high-dimensional KL and HFs. In particular, signatures of the gapped small Fermi surface (i.e., hybridization gap) should be visible in the charge sector in the weak-coupling, heavy-mass regime, as they are in one dimension.

ACKNOWLEDGMENTS. We thank Erez Berg, Sylvain Capponi, Anna Kesselman, and Daniel Podolsky for beneficial discussions. We also thank David Cohen for his extensive technical support. P.A. thanks the Physics Department of the Technion for their kind hospitality. C.H. and U.S. acknowledge funding through the Exploring Quantum Matter (ExQM) Graduate School of the Bavarian Elite Network and the Nanosystems Initiative Munich. A.A. acknowledges United States–Israel Binational Science Foundation Grant 2016168 and Israel Science Foundation Grant 1111/16 as well as the Kavli Institute for Theoretical Physics under National Science Foundation Grant NSF PHY-1125915 for its hospitality.

1. Kasuya T (1956) A theory of metallic ferro- and antiferromagnetism on Zener's model. *Prog Theor Phys* 16:45–57.
2. Doniach S (1977) The Kondo lattice and weak antiferromagnetism. *Physica B+C* 91:231–234.
3. Hewson AC (1993) *The Kondo Problem to Heavy Fermions*. Cambridge Studies in Magnetism (Cambridge Univ Press, Cambridge, UK).
4. Coleman P (1984) New approach to the mixed-valence problem. *Phys Rev B* 29:3035–3044.
5. Read N, Newns DM, Doniach S (1984) Stability of the Kondo lattice in the large-*N* limit. *Phys Rev B* 30:3841–3844.
6. Auerbach A, Levin K (1986) Kondo bosons and the Kondo lattice: Microscopic basis for the heavy Fermi liquid. *Phys Rev Lett* 57:877–880.
7. Millis AJ, Lee PA (1987) Large-orbital-degeneracy expansion for the lattice Anderson model. *Phys Rev B* 35:3394–3414.
8. Luttinger JM (1960) Fermi surface and some simple equilibrium properties of a system of interacting fermions. *Phys Rev* 119:1153–1163.
9. Yamanaka M, Oshikawa M, Affleck I (1997) Nonperturbative approach to Luttinger's theorem in one dimension. *Phys Rev Lett* 79:1110–1113.
10. Oshikawa M (2000) Topological approach to Luttinger's theorem and the Fermi surface of a Kondo lattice. *Phys Rev Lett* 84:3370–3373.
11. Tsunetsugu H, Sigrist M, Ueda K (1997) The ground-state phase diagram of the one-dimensional Kondo lattice model. *Rev Mod Phys* 69:809–864.
12. Taillefer L, Lonzarich GG (1988) Heavy-fermion quasiparticles in upt_3. *Phys Rev Lett* 60:1570–1573.
13. Aynajian P et al. (2012) Visualizing heavy fermions emerging in a quantum critical Kondo lattice. *Nature* 486:201–206.
14. Ruderman MA, Kittel C (1954) Indirect exchange coupling of nuclear magnetic moments by conduction electrons. *Phys Rev* 96:99–102.
15. Houghton A, Read N, Won H (1987) 1/N expansion for the transport coefficients of the single-impurity Anderson model. *Phys Rev B* 35:5123–5150.
16. Yang Yf, Fisk Z, Lee HO, Thompson JD, Pines D (2008) Scaling the Kondo lattice. *Nature* 454:611–613.
17. Sikkema AE, Affleck I, White SR (1997) Spin gap in a doped Kondo chain. *Phys Rev Lett* 79:929–932.
18. Zachar O (2001) Staggered liquid phases of the one-dimensional Kondo-Heisenberg lattice model. *Phys Rev B* 63:205104.
19. Berg E, Fradkin E, Kivelson SA (2010) Pair-density-wave correlations in the Kondo-Heisenberg model. *Phys Rev Lett* 105:146403.
20. Shibata N, Ueda K, Nishino T, Ishii C (1996) Friedel oscillations in the one-dimensional Kondo lattice model. *Phys Rev B* 54:13495–13498.
21. McCulloch IP, Juozapavicius A, Rosengren A, Gulacsi M (2002) Localized spin ordering in Kondo lattice models. *Phys Rev B 65*:052410.
22. Peters R, Kawakami N (2012) Ferromagnetic state in the one-dimensional Kondo lattice model. *Phys Rev B* 86:165107.
23. Sigrist M, Tsunetsugu H, Ueda K, Rice TM (1992) Ferromagnetism in the strong-coupling regime of the one-dimensional Kondo-lattice model. *Phys Rev B* 46:13838–13846.
24. Tsunetsugu H, Hatsugai Y, Ueda K, Sigrist M (1992) Spin-liquid ground state of the half-filled Kondo lattice in one dimension. *Phys Rev B* 46:3175–3178.
25. Troyer M, Würtz D (1993) Ferromagnetism of the one-dimensional Ksondo-lattice model: A quantum Monte Carlo study. *Phys Rev B* 47:2886–2889.
26. Ueda K, Tsunetsugu H, Sigrist M (1993) Phase diagram of the Kondo lattice model. *Phys B Condens Matter* 186:358–361.
27. Shibata N, Ueda K (1999) The one-dimensional Kondo lattice model studied by the density matrix renormalization group method. *J Phys Condens Matter* 11:4289–4290.
28. White SR (1992) Density matrix formulation for quantum renormalization groups. *Phys Rev Lett* 69:2863–2866.
29. Shibata N, Tsvelik A, Ueda K (1997) One-dimensional Kondo lattice model as a Tomonaga-Luttinger liquid. *Phys Rev B* 56:330–334.
30. Haldane FDM (1981) 'Luttinger liquid theory' of one-dimensional quantum fluids. I. Properties of the Luttinger model and their extension to the general 1D interacting spinless Fermi gas. *J Phys C Solid State Phys* 14:2585–2609.
31. Giamarchi T (2004) *Quantum Physics in One Dimension* (Oxford Univ Press, Oxford), Vol 121.
32. Xavier J, Novais E, Miranda E (2002) Small Fermi surface in the one-dimensional Kondo lattice model. *Phys Rev B* 65:214406.
33. Xavier JC, Miranda E (2004) Correlation exponent K_ρ of the one-dimensional Kondo lattice model. *Phys Rev B*70:075110.
34. Tsvelik A, Yevtushenko O (2015) Quantum phase transition and protected ideal transport in a Kondo chain. *Phys Rev Lett* 115:216402.
35. Schimmel DH, Tsvelik AM, Yevtushenko OM (2016) Low energy properties of the Kondo chain in the rkky regime. *New J Phys* 18:053004.
36. White SR, Affleck I, Scalapino DJ (2002) Friedel oscillations and charge density waves in chains and ladders. *Phys Rev B* 65:165122.
37. Auerbach A, Levin K (1987) The Anderson lattice and universal properties of heavy fermion systems. *Theoretical and Experimental Aspects of Valence Fluctuations and Heavy Fermions*, eds Gupta LC, Malik SK (Springer, Boston), pp 495–499.
38. White SR, Affleck I (1996) Dimerization and incommensurate spiral spin correlations in the zigzag spin chain: Analogies to the Kondo lattice. *Phys Rev B* 54:9862–9869.
39. White SR, Feiguin AE (2004) Real-time evolution using the density matrix renormalization group. *Phys Rev Lett* 93:076401.
40. Daley AJ, Kollath C, Schollwöck U, Vidal G (2004) Time-dependent density-matrix renormalization-group using adaptive effective hilbert spaces. J Stat Mech Theor Exp 2004:P04005.
41. Xavier JC, Pereira RG, Miranda E, Affleck I (2003) Dimerization induced by the RKKY interaction. *Phys Rev Lett* 90:247204.